International Journal of Heat and Mass Transfer 51 (2008) 5288–5295

Contents lists available at ScienceDirect

International Journal of Heat and Mass Transfer

journal homepage: www.elsevier.com/locate/ijhmt

A fractal model for gas permeation through porous membranes

Li-Zhi Zhang *

Key Laboratory of Enhanced Heat Transfer and Energy Conservation of Education Ministry, School of Chemistry and Chemical Engineering, South China University of Technology, Guangzhou 510640, China

ARTICLE INFO

Article history:
Received 23 July 2007
Revised in revised form 8 January 2008
Available online 5 May 2008

Keywords:
Fractal
Permeability
Gas permeation
Porous membranes

ABSTRACT

Macro and micro porous membranes have been used in many industrial areas. The disordered nature of pore structures in these membranes suggests the existence of a fractal structure formed by the pores. Fractal theory is employed to build the permeation model through these porous membranes. The fractal dimensions for surface pore area and tortuosity of membrane is obtained by box-counting method. Contrary to previous studies which consider only the Poiseulle flow in pores, in this research, the model reflects two gas diffusion mechanisms simultaneously: when the Knudsen number is less than 0.01, the Poiseulle flow is dominant; while when the Knudsen number is greater than 10, the Knudsen flow is dominant; and when the Knudsen number is from 0.01 to 10, the two mechanisms coexist. Contact gas permeation experiments with three porous hydrophobic PVDF membranes are conducted to validate the model. Comparisons between the current model and those from references are made.

1. Introduction

Porous membranes have been used in many areas, such as ultrafiltration, pervaporation, and distillation. Besides, they were extensively used in gas separations, in which a thin dense permselective active layer is usually fabricated on a porous support layer. The porous support membrane ensures the high permeability, and the necessary mechanical strength.

Modeling of mass (gas or vapor) transfer through the membrane pores has received much attention from various investigators [1,2]. Khayet and Matsuura [3] investigated the effects of mean pore size, porosity, and pore size distribution on gas diffusion in membrane distillation processes. Martinez et al. [4] studied the pore size distribution for three hydrophobic porous membranes, and modeled water vapor permeabilities, to name but a few examples. Since the microstructures of the porous media are usually disordered and extremely complicated, this makes it very difficult to analytically find the permeability. In order to get a better understanding of the mechanisms for permeability, the analytical solution for permeability of porous membrane becomes a challenging task.

Figs. 1 and 2 show the scanning electron micrograph (SEM) pictures for two typical porous membranes, Nylon and Mixed Cellulose, respectively. Their nominal pore diameters are 0.15 μm and 0.8 μm, respectively. The disordered nature of pore structures in these porous membranes suggests the existence of a fractal structure formed by the macro and micro pores. These pores and their distributions are analogous in the microstructure to pores in sandstone, to islands or lakes on earth. Therefore, it is possible to obtain the permeability of porous membranes through a fractal analysis on pore microstructures [5].

Fractal theory is a new theory to analyzing natural phenomenon, which allows the characterization of objects in terms of their self-similar (scale invariant) properties (i.e., parts of the object are similar to the whole after rescaling) [6]. Fractal techniques have been used in diverse engineering applications that involve physical phenomena in disordered structures and over multiple scales [6,7]. In all these applications, the fractal dimensions have been very effective in making complex structures easy for analysis, and it is this capability that inspires the current study to perform fractal analysis on membrane structures.

There have been several studies of fractal analysis for porous media. Pitchumani and Ramakrishnan [7] proposed a fractal geometry model for evaluating permeabilities of porous performs used in liquid composite molding. However, their model presents the contradictory results with fractal geometry theory, see the comments by Yu [8] for detail. Yu and Cheng [9] further developed a fractal permeability model for bi-dispersed porous media, in terms of the tortuosity fractal dimension, pore area fractal dimension, and porosities of the medium. Yu and Lee [10] then developed fractal permeability models for both saturated and unsaturated porous media. In a subsequent series of work, Yu and co-workers further developed fractal models for other porous media like fabrics [11–13]. Recently, they also used Monte Carlo simulations to study the permeability of fractal porous media [14].

As for the fractal analysis of membranes, Meng et al. [15] applied the fractal permeation model to investigate membrane

* Tel./fax: +86 20 87114268.
E-mail address: Lzzhang@scut.edu.cn

0017-9310/$ - see front matter © 2008 Elsevier Ltd. All rights reserved.
doi:10.1016/j.ijheatmasstransfer.2008.03.008

Nomenclature

A_c	cross section area (m^2)
A_t	transfer area (m^2)
d	diameter of membrane fiber (m)
D_{eff}	effective diffusivity (m^2/s)
D_f	area fractal dimension
D_f	tortuosity fractal dimension
D_{va}	moisture diffusivity in dry air (m^2/s)
H_d	duct height (m)
K	total mass transfer coefficient (m/s)
k_B	Boltzmann constant, 1.38×10^{-23} J/K
Kn	Knudsen number
k_s	convective mass transfer coefficient (m/s)
L	length scale (m)
L_0	representative length of a straight capillary (m)
l_s	length of the cell space (m)
M	mole molecule weight (kg/mol)
N	number of pores
P	total pressure (Pa)
p_A	partial pressure of gas A (Pa)
Pe	permeability (m^2)
q	gas flow through a single pore (m^3/s)
Q	total gas flow through a membrane (m^3/s)
R	gas constant (8.314J mol^{-1} K^{-1})
Sh	Sherwood number
T	temperature (K)

Greek symbols

λ	pore diameter (m)
μ	viscosity (Pa s)
ρ	density (kg m^{-3})
ω	humidity ratio (kg/kg)
τ	mean free path (m)
σ	molecular collision diameter (m)
ε	porosity

Subscripts

A	gas A
B	gas B
K	Knudsen
m	mean
P	Poiseulle

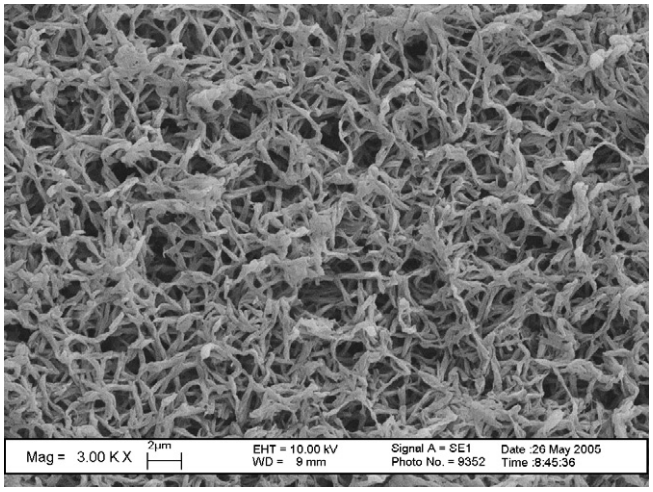

Fig. 1. SEM graph of a nylon porous membrane, nominal pore size 0.15 μm.

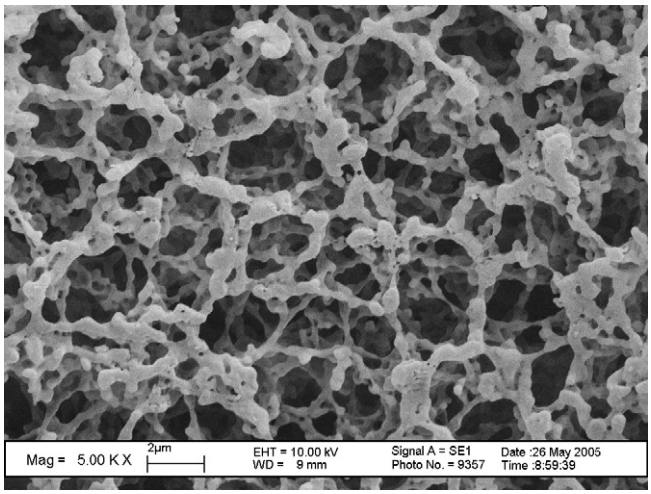

Fig. 2. SEM graph of a mixed cellulose porous membrane, nominal pore size 0.8 μm.

fouling in membrane bioreactors. Recently, He et al. [16] used a fractal model to predict the permeability in gas diffusion layer of proton exchange membrane fuel cells.

In all these fractal model developments, mass flow in the pores is assumed in Poiseulle flow regime. However, in porous membranes, it is believed that Poiseulle flow is predominant only when Knudsen number (the ratio of gas mean free path to pore diameter) is less than 0.01 [4,17]. When the Knudsen number is greater than 10, on the other hand, Knudsen diffusion is predominant [4,17]. As a result, the previous fractal models are not appropriate for gas diffusion in porous membranes which has a wide pore size distribution. It is therefore necessary to develop a new fractal model for gas or vapor permeations in porous membranes.

2. Mathematical model

2.1. Fractal characteristics of porous membrane

The measure of a fractal structure $M(L)$ is related to the length scale L, through a power law in the form of

$$M(L) \sim L^{D_f} \tag{1}$$

where '$\sim$' means 'scale as', and D_f is the fractal dimension. Porous membrane has numerous pores with various sizes in the membrane, and can be considered as a bundle of tortuous capillary tubes with variable radius for the two-dimensional case. Let the diameter of a capillary tube be λ, and its tortuous length along the flow direction be $L(\lambda)$. The relationship between them exhibits the fractal scaling law [7,9]

$$\frac{L(\lambda)}{L_0} = \left(\frac{L_0}{\lambda}\right)^{D_t - 1} \tag{2}$$

where L_0 is the representative length of a straight capillary, which is equal to membrane thickness. D_t is the tortuosity dimension, with $1 \leqslant D_t \leqslant 2$. Large value of D_t within this range corresponds to a highly tortuous capillary, while $D_t = 1$ denotes a straight capillary pathway, $D_t = 2$, corresponds to a highly tortuous line that fills a plane.

The relationship between the number of pores and the pore size λ is another important property of fractals. The pores in a porous

medium are analogous to the islands or lakes on the earth. The cumulative size distribution of them follows the power law relation [7,9]

$$N(L \geqslant \lambda) = \left(\frac{\lambda_{\max}}{\lambda}\right)^{D_f} \tag{3}$$

where $N(L \geqslant \lambda)$ represents the total number of pores with diameter greater than λ on unit cell $A_0(=L_0^2)$, $\lambda_{\max}$ is the maximum pore diameter. From Eq. (3), the total pore number can be expressed by

$$N_t(L \geqslant \lambda_{\min}) = \left(\frac{\lambda_{\max}}{\lambda_{\min}}\right)^{D_f} \tag{4}$$

and

$$-dN = D_f \lambda_{\max}^{D_f} \lambda^{-(D_f+1)} d\lambda \tag{5}$$

The negative sign in Eq. (5) implies that the pore number decreases with the increase of pore size. Eqs. (1)–(5) hold true for both exactly and statistically self-similar fractal geometries. For two-dimensional space, $1 \leqslant D_f \leqslant 2$. By combining Eqs. (4) and (5) we have

$$-\frac{dN}{N_t} = D_f \lambda_{\min}^{D_f} \lambda^{-(D_f+1)} d\lambda = f(\lambda) d\lambda \tag{6}$$

where $f(\lambda)$ is the probability density function.

Based on the normalization condition, the following equation should be satisfied [9]

$$\int_{-\infty}^{+\infty} f(\lambda) d\lambda = \int_{\lambda_{\min}}^{\lambda_{\max}} f(\lambda) d\lambda = 1 - \left(\frac{\lambda_{\min}}{\lambda_{\max}}\right)^{D_f} = 1 \tag{7}$$

The above equation equals unity if and only if [9]

$$\left(\frac{\lambda_{\min}}{\lambda_{\max}}\right)^{D_f} = 0 \tag{8}$$

The above equation implies that the statistically self-similar properties exist in porous media in the range of $\lambda_{\min} \sim \lambda_{\max}$ [9]. It should be noted that there might exist multi-fractals with different fractal dimensions in different ranges of scales for porous media. For those membranes that have relative uniform pore sizes, the fractal theory is not appropriate to use. Fortunately, most porous membranes have wide pore size distributions. For instance, the polytetrafluoroethylene (PTFE), polypropylene (PP) and polyvinylidene fluoride (PVDF) membranes used for membrane distillation have a pore size distribution from 0.01 μm to 1 μm [4].

2.2. Fractal model for permeability

The governing quantity that provides a guideline in determining which mechanism is operative in a given pore under given operating conditions is the ratio of the pore size to the mean free path τ, which is calculated for a species i using the following expression [17]:

$$\tau_i = \frac{k_B T}{\sqrt{2}\pi\sigma_i^2 P_m} \tag{9}$$

where σ_i is the molecular collision diameter of ith gas (m), 2.641 Å and 3.711 Å for water vapor and air, respectively [17]; k_B is the Boltzmann constant, 1.38×10^{-23} J/K, P_m is the mean total pressure within the membrane pores (Pa), and T is the absolute temperature (K).

For gaseous mixtures of two components A and B, the mean free path and the collision diameters are different from the corresponding quantities for the pure component. The following relationship can be applied for gas mixtures:

$$\sigma_{AB} = \frac{\sigma_A + \sigma_B}{2} \tag{10}$$

Under room temperature and atmospheric pressure, calculated τ for air is 0.07 μm; while under vacuum conditions, mean free path for air may be several microns to several meters. Obviously, operating conditions have a great influence on diffusion mechanisms.

The Knudsen number is defined by

$$Kn = \frac{\tau}{\lambda} \tag{11}$$

When $Kn < 0.01$, i.e., the pore size is large in relation with the mean free path of gas molecules, the molecule–molecule collisions between gas molecules themselves will dominate and viscous Poisseuille flow will occur. Under this mechanism, the gas flow through a single pore, $q(\lambda)$ (m^3/s), governed by the well-known Hagen–Poiseulle equation is [17]

$$q_P(\lambda) = \frac{\pi \Delta p_A}{128\mu} \frac{\lambda^4}{L(\lambda)} \tag{12}$$

where μ is the viscosity of permeation gas A (Pas), Δp_A is the transmembrane partial pressure difference for gas A (Pa).

For a relatively small pore size, $Kn \geqslant 10$, if the mean free path of the gas molecules is large in relation with the pore size, the molecule–pore wall collisions are dominant over the molecule–molecule collisions and the gas transport takes place via Knudsen flow. In this case, one obtains the following relationship for the gas flow in a single pore [17]:

$$q_K(\lambda) = \frac{\pi\lambda^3}{12 p_{Am}} \sqrt{\frac{8RT}{\pi M_A}} \frac{\Delta p_A}{L(\lambda)} \tag{13}$$

where p_{Am} is the mean partial pressure of diffusion gas A (Pa) in pores, M_A is the molecule weight of gas A (kg/mol); R is gas constant, 8.314 J/(mol K).

Between the two limits of Knudsen diffusion and Poisseuille flow, i.e., $0.01 \leqslant Kn < 10$, the above mentioned two mechanisms may coexist. The Knudsen resistance and viscous resistance will be combined like resistors in parallel [4], then the combined flow is

$$q_{PK} = q_P + q_K \tag{14}$$

In the case of a membrane with a pore size distribution, all the above mechanisms may exist, but to different extents, depending on the operating conditions and membrane morphological characteristics. Finally, considering the various diameters of pores in the membrane, the gas flux across the membrane, Q, is

$$Q = -\int_{\lambda_{\min}}^{\lambda_K} q_K dN(\lambda) - \int_{\lambda_K}^{\lambda_P} q_{PK} dN(\lambda) - \int_{\lambda_P}^{\lambda_{\max}} q_P dN(\lambda) \tag{15}$$

where characteristic pore diameter λ_K and λ_P are defined based on Knudsen number as

$$\lambda_K = 0.1\tau \tag{16}$$

$$\lambda_P = 100\tau \tag{17}$$

Substituting Eqs. (5) and (8) into Eq. (15), and the integration of the first term gives

$$Q_K = \frac{\pi D_f \lambda_{\max}^{D_f} \Delta p_A}{12 p_{Am} L_0^{D_t} (2 + D_t - D_f)} \sqrt{\frac{8RT}{\pi M_A}} \lambda_K^{2-D_f+D_t} \tag{18}$$

The integration of the second term gives

$$Q_{PK} = \frac{\pi D_f \lambda_{\max}^{D_f} \Delta p_A}{12 p_{Am} L_0^{D_t} (2 + D_t - D_f)} \sqrt{\frac{8RT}{\pi M_A}} \left[\lambda_P^{2-D_f+D_t} - \lambda_K^{2-D_f+D_t}\right] + \frac{\pi D_f \lambda_{\max}^{D_f} \Delta p_A}{128\mu L_0^{D_t} (3 + D_t - D_f)} \left[\lambda_P^{3-D_f+D_t} - \lambda_K^{3-D_f+D_t}\right] \tag{19}$$

The integration of the last term is

$$Q_P = \frac{\pi D_f \lambda_{max}^{D_f} \Delta p_A}{128 \mu L_0^{D_t} (3 + D_t - D_f)} \left[\lambda_{max}^{3-D_f+D_t} - \lambda_P^{3-D_f+D_t} \right] \quad (20)$$

The permeability (m^2) can be expressed as follows according to the Darcy's law

$$Pe = \frac{\mu L_0 Q}{\Delta p_A A_0} \quad (21)$$

where $A_0 = L_0^2$ is the unit membrane area.

Substituting A_0, and Eqs. (18)–(21), the permeability is then deduced to

$$Pe = \frac{\pi D_f L_0^{-1-D_t} \lambda_{max}^{D_f}}{128(3 + D_t - D_f)} \left(\lambda_{max}^{3-D_f+D_t} - \lambda_K^{3-D_f+D_t} \right) + \frac{\pi \mu L_0^{-1-D_t} D_f \lambda_{max}^{D_f}}{12 p_{Am} (2 + D_t - D_f)} \sqrt{\frac{8RT}{\pi M_A}} \left(\lambda_P^{2-D_f+D_t} \right) \quad (22)$$

This is the fractal model developed.

Gas effective diffusivity D_{eff} (m^2/s) through membrane is another important parameter. By considering ideal gas state equation

$$p_A = \frac{\rho_A RT}{M_A} \quad (23)$$

The relation between diffusivity and permeability is

$$D_{eff} = \frac{Pe \cdot RT}{\mu M_A} \quad (24)$$

The situations of gas permeation through dense membranes (pore size < 2 nm), which rely on solution-diffusion mechanisms, and the interactions between the gas and membranes, are not considered in this model.

3. Experiment

3.1. Test rig

A test rig has been set-up to measure the vapor permeability in porous membranes. The test is used to validate the fractal model. To neglect the effect of vapor sorption by membrane (the interactions between the membrane and vapor), a hydrophobic porous membrane PVDF is used. The whole test set-up is shown in Fig. 3. Two air streams, one humid (air stream 1) and one dry (air stream 2), flow through a membrane exchanger to exchange moisture. For the humid strip, ambient air is humidified and is driven to a heating/cooling coil in a hot/cool water bath. After the temperature and humidity reach test conditions, the air is then drawn through the exchanger for moisture exchange. For the dry stream, it is driven directly from ambient to the exchanger. The two inlets temperatures are set to the same values. The composite membrane is sandwiched by two stainless steel half shells. Two parallel air passages on both sides of membrane are formed, which is like a counter-flow one-plate plate-and-shell heat exchanger. A schematic of the membrane exchanger is shown in Fig. 4. The flow channel height is 2 mm, and both the width and length are 10 cm. The effective membrane area is 100 cm^2. The SEM graph of the PVDF membrane is shown in Fig. 5, in which (a) shows the surface and (b) shows the cross section. The system simulates a contact membrane gas permeation process. Water vapor will permeate through the membrane pores from the humid air side to the dry air side, under partial vapor differences. The characteristic parameters for the membrane (MEM1) are: thickness 100 μm, nominal pore size 0.15 μm, porosity 0.78.

To have a balanced flow, equal air flow rates are kept for the two air streams. The uncertainties are: temperature ±0.1 °C; humidity ±1%; volumetric flow rate ±1%. The final uncertainty is ±4.5%.

The operating conditions for the tests are: stream 1 inlet, 25 °C, 80%RH; stream 2 inlet, 25 °C, 40%RH, air flow rates, 24 L/min.

3.2. Data reduction

The moisture transfer in the exchanger is governed by three resistances: the boundary layer resistance on humid air side, the membrane resistance, and the boundary layer resistance on dry air side. For convenience, a total mass transfer coefficient K is used to summarize the moisture transfer through the membrane. It summarizes the above three resistance simultaneously [18].

$$\frac{1}{K} = \frac{2}{k_s} + \frac{L_0}{D_{eff}} \quad (25)$$

where k_s is the convective mass transfer coefficient (m/s) between air stream and membrane on two sides. Convective mass transport in the channel can be represented by fully developed laminar flow in duct of parallel-plates cross section and is calculated by [19]

$$Sh = 7.54 \quad (26)$$

where Sh is Sherwood number, and is defined by

$$Sh = \frac{2 k_s H_d}{D_{va}} \quad (27)$$

where H_d is duct height (m) and D_{va} is moisture diffusivity in dry air (m^2/s).

After the inlet and outlet humidity are measured, the total mass transfer coefficients are calculated by

$$K = \frac{u_a A_c (\omega_{1i} - \omega_{1o})}{A_t \Delta \omega_{lm}} \quad (28)$$

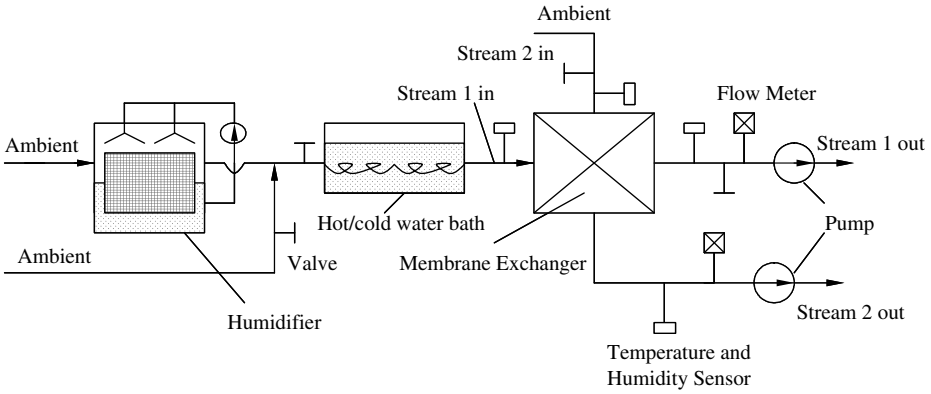

Fig. 3. Experimental set-up.

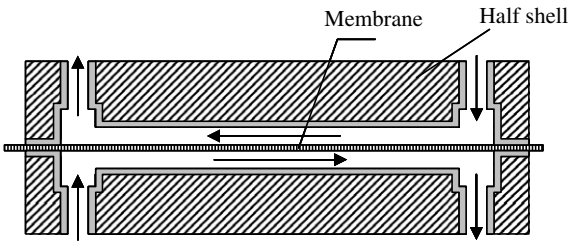

Fig. 4. Structure of the membrane exchanger comprised by two symmetric half cells.

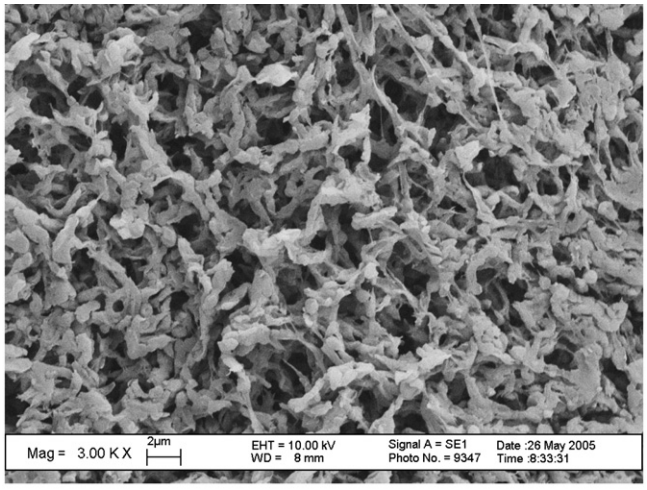

(a) Surface

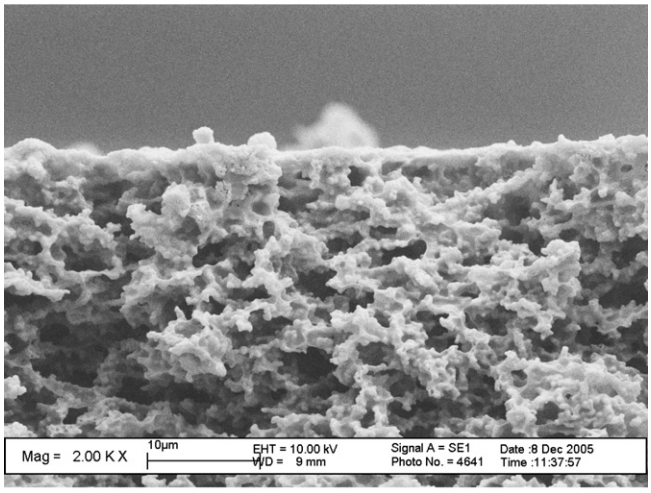

(b) Cross section

Fig. 5. SEM graph of the PVDF membrane used.

where A_c is the cross section area of air duct (m^2), A_t is the transfer area of membrane in the cell (m^2), $\Delta\omega_{lm}$ is the logarithmic mean humidity difference between the two air streams, and it is calculated by

$$\Delta\omega_{lm} = \frac{(\omega_{1i} - \omega_{2o}) - (\omega_{1o} - \omega_{2i})}{\ln\frac{(\omega_{1i} - \omega_{2o})}{(\omega_{1o} - \omega_{2i})}} \tag{29}$$

where ω represent humidity ratio (kg/kg); subscripts 1 and 2 represent air stream 1 and air stream 2 respectively; subscripts i and o represent inlet and outlet, respectively.

With outlet humidity and air flow rates, the total mass transfer coefficient can be obtained from Eq. (28). Then the effective diffusivity D_{eff} can be calculated by Eq. (25). Finally, permeability *Pe* can be obtained from Eq. (24). This is denoted as the experimentally obtained permeability. On the other hand, the *Pe* obtained from Eq. (22) is the one that comes from Fractal theory. By comparing these two Pes, we can compare the fitness and the applicability of the fractal theory.

4. Results and discussion

4.1. Determination of $\boldsymbol{D}_f$ and $\boldsymbol{D}_t$

The area dimension D_f can be determined by the box-counting method [7,9]. This method is based on the image analysis of a sufficiently large section on the membrane surface. According to this method, the membrane sample under consideration is discretized using square boxes of size *L*. Then the number, $N(L \geqslant \lambda)$, of boxes required to completely cover the pore areas is counted. The pore area fractal dimension, D_f, can be determined by the value of the slope of a linear fit through data on a logarithmic plot of the cumulative number of pores $N(L \geqslant \lambda)$ verses the square box size *L*.

Images acquired using SEM are JEPG format coded with true color. Images were transferred to gray-scale formation (256 gray-scale levels) with Adobe Photo 7.0 software. Before analyzing an image, a threshold has to be determined in order to distinguish pores from the background, obtaining a binary image. For each binary image, threshold was estimated as the gray level that corresponded to that maximum of the gray level histogram second derivation [15]. The pore area value can be determined by accumulating the binary images. The method simultaneously calculates the pore size distributions of $N(\lambda) \sim \lambda$.

The SEM images are magnified with 3000, as shown in Fig. 5a. The number of pores which is completely covered by a box of size *L* is counted. Then the logarithmic plot of the cumulative number of pores verses box size *L* for the membrane surface is plotted in Fig. 6a. As seen, the number of cumulative pores increases as the box size increases. The data follow an ideal linear relationship on the logarithmic scale, and this confirms the statistical fractal nature of the microstructures of the porous membrane. From the slope, we can determine the fractal dimensions $D_f = 1.94$.

The SEM graph of the cross section of the PVDF membrane is shown in Fig. 5b. In membrane SEM observations, the cross sectional samples are not prepared with microtome. The reason is that the membranes are rather thin, in the order of 100. μm. On the contrary, they are prepared in the following way: (1) the membrane is frozen in liquid nitrogen; (2) The membrane is fractured in the liquid nitrogen; (3) the exposed cross section is coated with gold; (4) the cross section is observed by SEM. The surface may be rough, but they are the real surface of a true sample, not just an ideal one.

It should be noted that the tortuosity itself is an approximate parameter to offset the zigzag nature of porous media. It is not a parameter that can be clearly and directly observed. In this study, since the tortuosity of the flow pathways is resulted from the convolution of the boundaries of the porous regions in membrane cross section, the tortuosity dimension may therefore be evaluated as the fractal dimension of the perimeter of the porous regions on cross section, which may also be obtained by the box-counting method mentioned above. The method has been proved successful in Ref. [16].

The logarithmic plot of the cumulative number of pores verses perimeter *L* on membrane cross section, i.e., $\log(N(L)) \sim \log(L)$ is shown in Fig. 6b. From this slope, it is determined that $D_t = 1.92$. It is highly tortuous, which is in accordance to the sponge-like structure in the membrane.

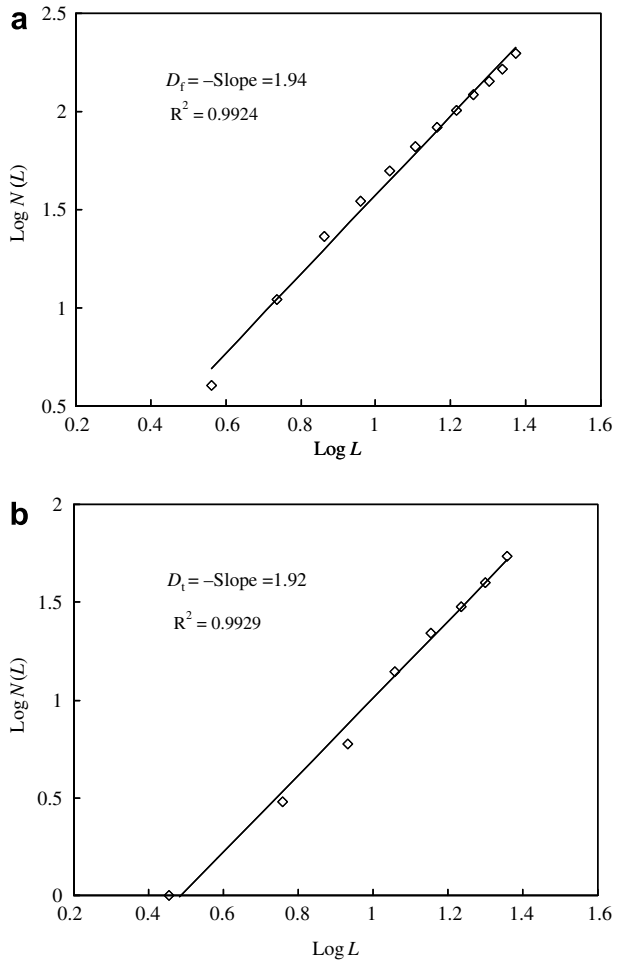

Fig. 6. Schematic illustration of the procedure for evaluation of fractal dimensions. (a) Area dimension D_f, (b) tortuosity dimension D_t.

4.2. Determination of λ_{max}

The maximum pore size in the permeability equation corresponds to the pore space formed between the membrane fibers. The membrane fiber matrix may be considered to be randomly packed ideally equi-spaced aligned fiber screens [16] as shown in Fig. 7. For this structure, the maximum pore space may be considered to be resulted from a single ordered membrane fiber screen according to the equation

$$\varepsilon = \frac{l_s^2}{(l_s + d)^2} \tag{30}$$

where l_s is the length of the space, and d is the diameter of a membrane fiber. According to the SEM graph shown in Fig. 5, the mean value of d is 1.2 μm, and the surface porosity of membrane is measured as 0.78. With known porosity and fiber diameter, space length can be calculated as 9.3 μm.

Then the maximum pore size can be

$$\lambda_{\max} = 2\sqrt{l_s^2/\pi} \tag{31}$$

The value for $\lambda_{\max}$ is 10.5 μm.

4.3. Validation of the permeability model

The permeability is very sensitive to maximum pore size. By varying the membrane's maximum diameters while setting other membrane parameters fixed, the model is used to calculate the variations of permeability with maximum pore size. The results are shown in Fig. 8. The calculated results with the model developed in Ref. [16] are also plotted in this figure. This model is proposed for a fuel cell membrane and is solely based on Poiseulle flow assumptions. The experimentally obtained permeability for MEM1 in Section 3.2 is also plotted in this figure. Generally speaking, the current model predicts the experiment well. In comparison, the model in Ref. [16] underestimates the experiment by six folds. The two models are in agreement when the maximum pore size exceeds 15 μm. The smaller the maximum pore size is, the larger the disparity between the two models is. This is because the smaller the pore size is, the more predominant the Knudsen flow is and the less dominant the Poiseulle flow is. The calculated pore size distribution for this membrane based on Eq. (5) is shown in Fig. 9. As seen, the pore numbers for a given pore diameter (-dN) decreases drastically as pore size increases. Most of the pores are in smaller diameters. They will dominate the mass transfer. It is observed from this figure that pores with diameters larger than 7 μm (in Poiseulle flow regime) only account for a small proportion, while pores in transitional flow regime ($0.07 \leqslant \lambda \leqslant 7$ μm) and Knudsen flow regime ($\lambda \leqslant 0.07$ μm) account for the largest proportion. Therefore, Knudsen flow is predominant.

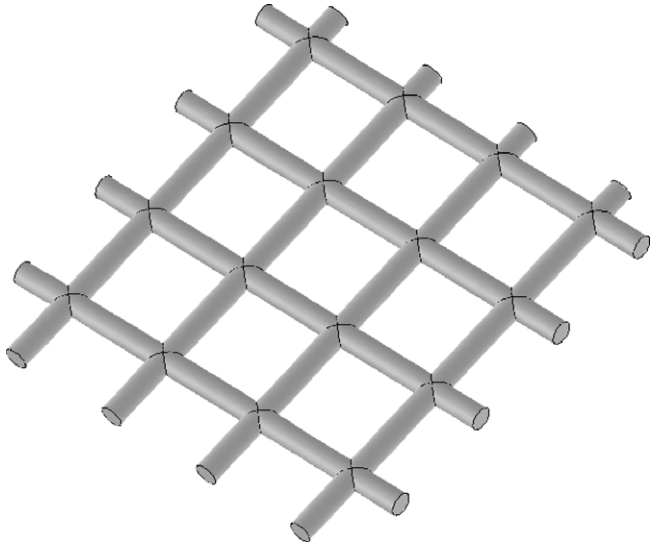

Fig. 7. An ideal membrane fiber matrix.

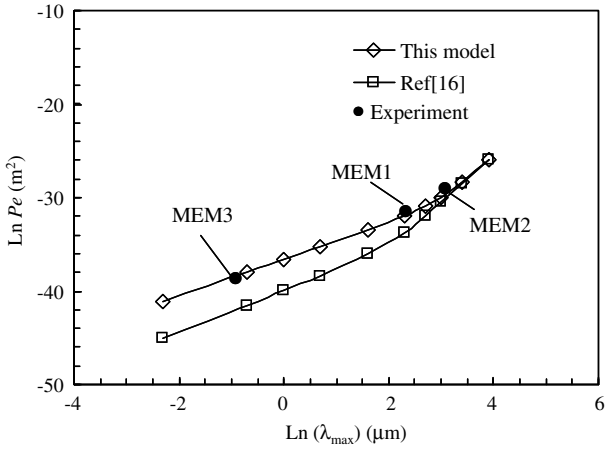

Fig. 8. Predicted permeability with various maximum pore size.

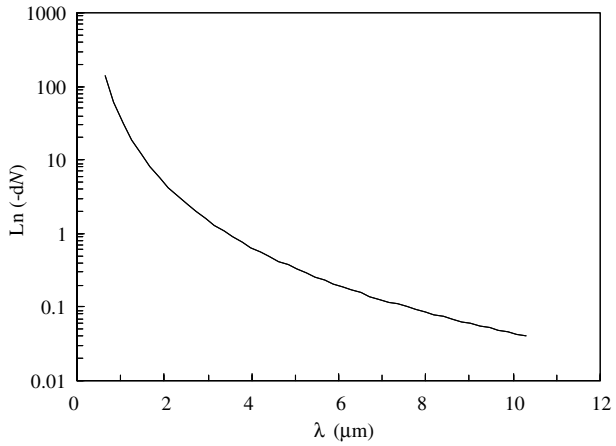

Fig. 9. Pore size distribution on the membrane, λ_{max} = 10.5 μm.

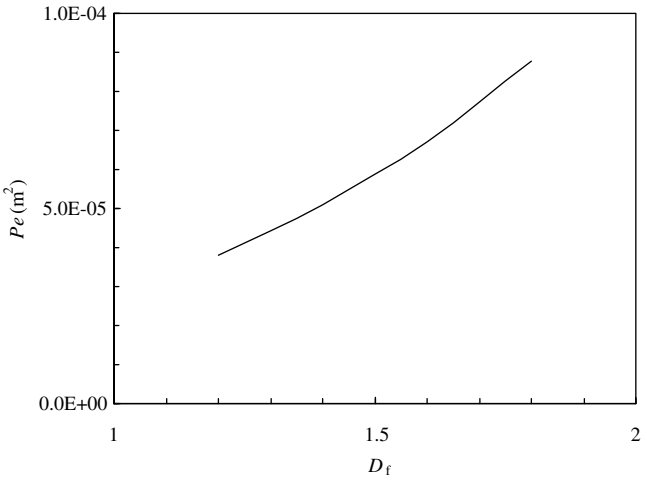

Fig. 10. Effects of surface area fractal dimension D_f on permeability.

Table 1
Comparisons of permeability in each diffusion region

Membranes	Permeability (m^2)			
	Knudsen region	Transitional region	Poiseulle region	Total
Pores	$Kn \geqslant 10$	$0.01 \leqslant Kn < 10$	$Kn < 0.01$	
MEM1	5.0×10^{-16}	1.8×10^{-15}	1.0×10^{-16}	2.4×10^{-15}
MEM2	5.0×10^{-15}	1.22×10^{-13}	5.45×10^{-13}	6.72×10^{-13}
MEM3	3.33×10^{-17}	7.82×10^{-18}	4.98×10^{-18}	4.61×10^{-17}

To evaluate permeations through other membranes, the membrane described above is denoted as MEM1. Two other PVDF membranes are also tested and analyzed. Their parameters are: MEM2, thickness 100 μm, nominal pore size 1.2 μm, porosity 0.76; MEM3, thickness 100 μm, nominal pore size 0.05 μm, porosity 0.78. The tested permeability values are also plotted in Fig. 9. As seen, the predicted and tested results for these two membranes are also in agreement.

Table 1 lists the calculated permeability in each diffusion region for the three tested membranes. The total permeability is the sum of the three permeabilities. As seen, the larger the pore size, the more dominant the Poiesulle flow.

It is also observed from Fig. 9 that, when the maximum pore diameter is larger than 15 μm, the larger pores will increase substantially, and the Poiseulle flow will dominant. Though there are still many smaller pores that are in either Knudsen or transitional flow regime, larger pores (>7 μm) that are in Poiseulle flow regime will account for the major proportion of the total pore numbers. Consequently larger pores will dominate the mass transfer in membrane. Then the current model and model in Ref. [16] will converge together. The determinative factor for which mechanism is dominant is the pore size distribution in the membrane. Regretfully, previous models totally neglect the Knudsen flow in small pores.

4.4. Parametric studies

Using the developed model, parametric studies are conducted. The maximum pore diameter is fixed to 10.5 μm. The effects of surface fractal dimension D_f, on permeability is calculated and shown in Fig. 10. As seen, the permeability is highly sensitive to D_f. The higher the surface fractal dimension is, the higher the permeability is. The reason is that a higher D_f usually generates to a higher porosity, which then leads to higher permeability. It should be noted that a higher porosity does not necessarily mean a higher permeability. Other parameters like pore diameter, tortuosity also play major roles. However, in this parametric study, it is assumed that other parameters are kept unchanged.

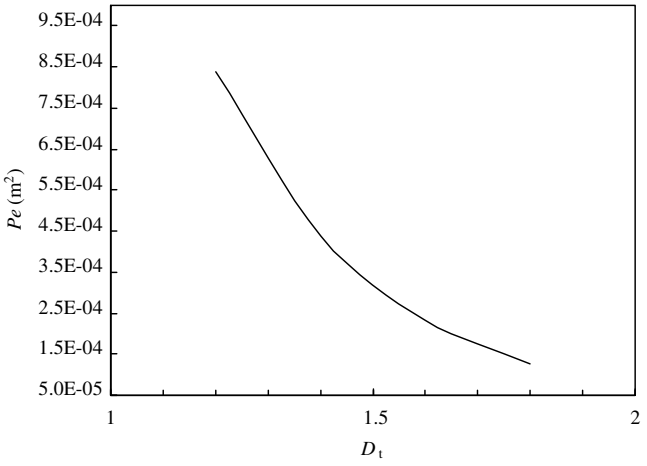

Fig. 11. Effects of tortuosity fractal dimension on permeability.

The effects of the tortuosity fractal dimension D_t on permeability are shown in Fig. 11. As seen, D_t has a rather great influence on permeability. The higher the fractal dimension is, the lower the permeability is. The reason is that a higher tortuosity means increased diffusion paths, which drastically increases diffusion resistances. These phenomena are in agreement with the experimental results from previous investigations on membrane applications [2–4].

5. Conclusions

A fractal gas diffusion model is proposed for prediction of permeability through macro and micro porous membranes. The model clarifies the gas diffusion mechanisms in the membrane pores: when the Knudsen number is less than 0.01, the Poiseulle flow is dominant; while when the Knudsen number is greater then 10, the Knudsen flow is dominant; and when the Knudsen number is from 0.01 to 10, the two mechanisms coexist. The numerical investigation and experimental validation found that the current model predicts the gas permeations in porous membranes well. In contrast, the previous model, which only considers Poiseulle flow, underestimates the permeability by 6 folds. Pore size distribution

has a determinative effect on which diffusion mechanism prevails. When the membrane maximum pore size exceeds 15 μm, the current model is in accordance to the available model from references. It provides a more accurate alternative methodology for gas permeation analysis in porous membranes.

The fractal model developed is necessary to build a relationship between the membrane structure and permeability. Certainly it may be not the only technique in permeation calculations, but it provides an efficient alternative, at least a trial, from a different perspective.

Acknowledgements

This Project 50676034 is supported by National Natural Science Foundation of China. The project is also partly supported by the National Key Project of Scientific and Technical Supporting Programs, No. 2006BAA04B02.

References

[1] E.A. Mason, A.P. Maulinaskas, Gas Transport in Porous Media: the Dusty Gas Model, Elsevier, Amsterdam, 1983.
[2] M. Khayet, P. Godino, J.I. Mengual, Nature of flow on sweeping gas membrane distillation, J. Membr. Sci. 170 (2000) 243–255.
[3] M. Khayet, T. Matsuura, Pervaporation and vacuum membrane distillation processes: modeling and experiments, AIChe J. 50 (2004) 1697–1712.
[4] L. Martinez, F.J. Florido-Diaz, A. Hernandez, P. Pradanos, Characterization of three hydrophobic porous membranes used in membrane distillation, modeling and evaluation of their water vapor permeabilities, J. Membr. Sci. 203 (2002) 15–27.
[5] C.E. Krohn, A.H. Thompson, Fractal sandstone pores: Automated measurements using scanning-electron-microscope images, Phys. Rev. B 33 (1986) 6366.
[6] B.B. Mandelbrot, The Fractal Geometry of Nature, Freeman, New York, 1982, p. 23.
[7] R. Pitchumani, B. Ramakrishnan, A fractal geometry model for evaluating permeabilities of porous performs used in liquid composite molding, Int. J. Heat Mass Transfer 42 (1999) 2219–2232.
[8] B.M. Yu, Comments on "A fractal geometry model for evaluating permeabilities of porous preforms used in liquid composite molding", Int. J. Heat Mass Transfer 44 (2001) 2787–2789.
[9] B. Yu, P. Cheng, A fractal permeability model for bi-dispersed porous media, Int. J. Heat Mass Transfer 45 (2002) 2983–2993.
[10] B.M. Yu, L.J. Lee, A fractal in-plane permeability model for fabrics, Polym. Compos. 23 (2002) 201–221.
[11] B.M. Yu, J.H. Li, D.M. Zhang, A fractal trans-plane permeability model for textile fabrics, Int. Commun. Heat Mass Transfer 30 (2003) 127–138.
[12] B.M. Yu, L.J. Lee, A simplified in-plane permeability model for textile fabrics, Polym. Compos. 21 (2000) 660–685.
[13] B.Y. Yu, W. Liu, Fractal analysis of permeabilities for porous media, AIChE J. 50 (2004) 46–56.
[14] B.M. Yu, M.Q. Zou, Y.J. Feng, Permeability of fractal porous media by Monte Carlo simulations, Int. J. Heat Mass Transfer 48 (2005) 2787–2794.
[15] F.G. Meng, H.M. Zhang, Y.S. Li, X.W. Zhang, F.L. Yang, Application of fractal permeation model to investigate membrane fouling in membrane bioreactor, J. Membr. Sci. 262 (2005) 107–116.
[16] G.L. He, Z.C. Zhao, P.W. Ming, A. Abuliti, C.Y. Yin, A fractal model for predicting permeability and liquid water relative permeability in the gas diffusion layer of PEMFCs, J. Power Sources 163 (2007) 846–852.
[17] E.L. Cussler, Diffusion–Mass Transfer in Fluid Systems, Cambridge University Press, 2000.
[18] L.Z. Zhang, J.L. Niu, Effectiveness correlations for heat and moisture transfer processes in an enthalpy exchanger with membrane cores, ASME J. Heat Transfer 122 (2002) 922–929.
[19] F.P. Incropera, D.P. Dewitt, Introduction to Heat Transfer, John Wiley & Sons, New York, 1996.